Kinetic Dissection of the Catalytic Mechanism of Taurine:α-Ketoglutarate Dioxygenase (TauD) from *Escherichia coli*†

John C. Price,‡ Eric W. Barr,‡ Lee M. Hoffart,‡ Carsten Krebs,*,‡,§ and J. Martin Bollinger, Jr.*,‡,§

Department of Biochemistry and Molecular Biology, and Department of Chemistry, The Pennsylvania State University, University Park, Pennsylvania 16802

Received February 7, 2005; Revised Manuscript Received March 28, 2005

ABSTRACT: Recent studies on taurine:α-ketoglutarate dioxygenase (TauD) from *Escherichia coli* have provided evidence for a three-step, minimal kinetic mechanism involving the quaternary TauD·Fe(II)·α-ketoglutarate·taurine complex, the taurine-hydroxylating Fe(IV)−oxo intermediate (**J**) that forms upon reaction of the quaternary complex with O_2, and a poorly defined, Fe(II)-containing intermediate state that converts in the rate-limiting step back to the quaternary complex [Price, J. C., Barr, E. W., Tirupati, B., Bollinger, J. M., Jr., and Krebs, C. (2003) *Biochemistry 42*, 7497−7508]. The mapping of this kinetic mechanism onto the consensus chemical mechanism for the Fe(II)- and α-ketoglutarate-dependent engendered several predictions and additional questions that have been experimentally addressed in the present study. The results demonstrate (1) that postulated intermediates between the quaternary complex and **J** accumulate very little or not at all; (2) that decarboxylation of α-ketoglutarate occurs prior to or concomitantly with formation of **J**; (3) that the second intermediate state comprises one or more product complex with Mössbauer features that are partially resolved from those of the binary TauD·Fe(II), ternary TauD·Fe(II)·α-ketoglutarate, and quaternary TauD·Fe(II)·α-ketoglutarate·taurine complexes; and (4) that the rate-determining step in the catalytic cycle is release of product(s) prior to the rapid, ordered binding of α-ketoglutarate and then taurine to regenerate the O_2-reactive quaternary complex. The results thus integrate the previously proposed kinetic and chemical mechanisms and indicate which of the postulated intermediates in the latter will be detectable only upon perturbation of the kinetics by changes in reaction conditions (e.g., temperature), protein mutagenesis, the use of substrate analogues, or some combination of these.

The Fe(II)- and α-ketoglutarate-dependent dioxygenases are a large family of enzymes (*1*) with roles in the biosynthesis of collagen (*2*), the cellular detection of and initiation of response to hypoxia (*3, 4*), the biosyntheses of antibiotic compounds (*5*−*7*), the repair of alkylated DNA (*8, 9*), and other biological processes. These enzymes couple the oxidative decarboxylation of α-ketoglutarate (αKG)[1] to the oxidation (mostly hydroxylation) of unactivated carbon atoms. Taurine:α-ketoglutarate dioxygenase (TauD) from *Escherichia coli*, a member of this family and the subject of the present study, hydroxylates C1 of taurine (2-aminoethane-1-sulfonic acid) and other organosulfonates, leading to elimination of sulfite and thereby initiating the acquisition of sulfur from compounds that contain the element in a form that would otherwise be biologically inert (*10*).

Members of the family to which TauD belongs employ a conserved $His_2(Asp/Glu)_1$-coordinated Fe(II) active site motif and are presumed to share a common chemical mechanism (*11, 12*) (shown in Scheme 1, adapted for the specific case of TauD). This mechanism, first proposed more than two decades ago (*13*), involves several chemically plausible intermediates. However, until recently, no direct evidence for any of these species had been reported. Recently, stopped-flow absorption and freeze-quench Mössbauer experiments on TauD provided the first direct demonstration of an oxidized iron intermediate (hereafter denoted **J**) in O_2 activation by a member of this family (*14*). A three-step, minimal kinetic mechanism for the TauD catalytic cycle, involving the reactant TauD·Fe(II)·αKG·taurine quaternary complex, **J**, and a poorly defined Fe(II)-containing, second intermediate state, was formulated. The subsequent demonstration of a large deuterium kinetic isotope effect on decay of **J** upon substitution of C1 of taurine suggested that **J** is the long-postulated, substrate-hydroxylating Fe(IV)−oxo complex (*15*), a suggestion later confirmed by resonance Raman and EXAFS characterization of the intermediate (*16, 17*).

The combined kinetic and spectroscopic data allow the minimal kinetic mechanism to be mapped onto the consensus

† This work was supported by start-up funds from the Pennsylvania State University (C.K.) and NIH Grant GM 69657 (C.K. and J.M.B.).

* To whom correspondence should be addressed. J. Martin Bollinger, Jr., Department of Biochemistry and Molecular Biology, 208 Althouse Laboratory, University Park, PA 16802; phone, 814-863-5707; fax, 814-863-7024; e-mail, jmb21@psu.edu. Carsten Krebs, Department of Biochemistry and Molecular Biology, 306 S. Frear Bldg., University Park, PA 16802; phone, 814-865-6089; fax, 814-863-7024; e-mail, ckrebs@psu.edu.

‡ Department of Biochemistry and Molecular Biology.

§ Department of Chemistry.

[1] Abbreviations: TauD, taurine:α-ketoglutarate dioxygenase; αKG, α-ketoglutarate or 2-oxo-1,5-pentanedioic acid; NMR, nuclear magnetic resonance; δ, Mössbauer isomer shift; ΔE_Q, Mössbauer quadrupole splitting; MS, mass spectrometry; HRMS, high-resolution mass spectrometry; ϵ, molar absorptivity; buffer A, 50 mM Tris·HCl, pH 7.6; RV, relative viscosity.

10.1021/bi050227c CCC: $30.25
Published on Web 05/13/2005

Scheme 1: Mapping of the Minimal Kinetic Mechanism for TauD Presented in Ref *14* onto the Current Working Hypothesis for the Chemical Mechanism[a]

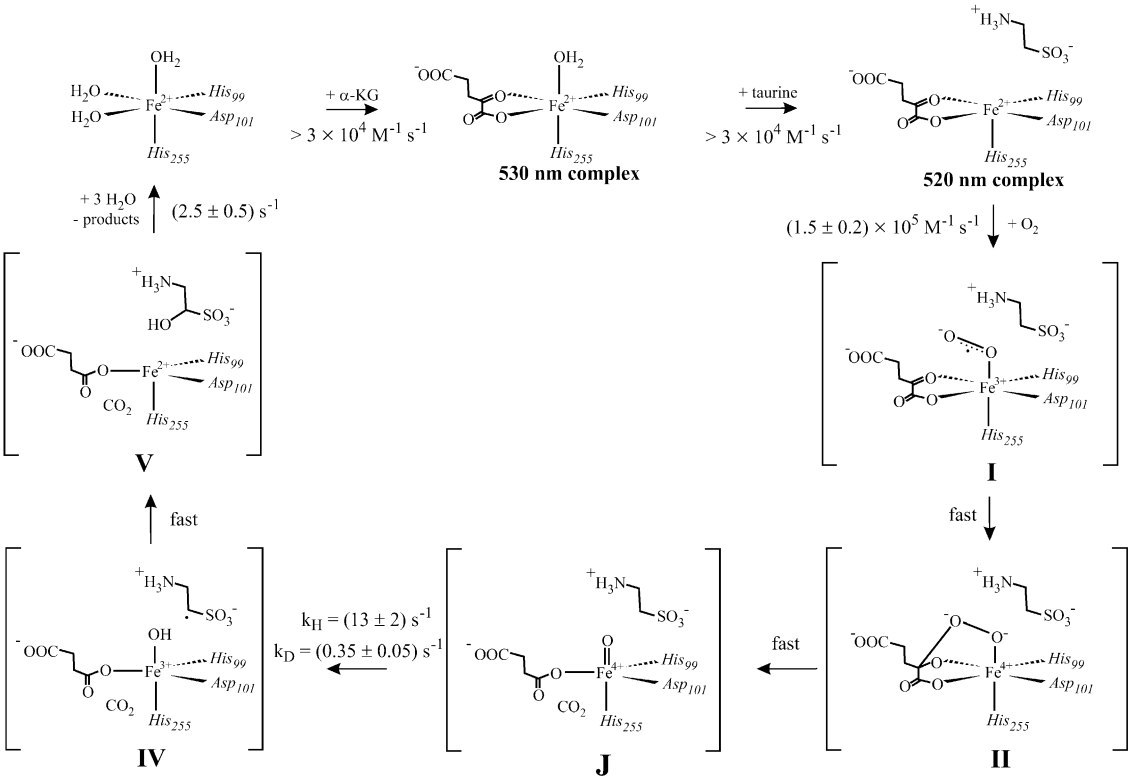

[a]The assignment of rate constants to individual steps relies on results from this work and from refs *14*−*17*. The rate constants refer to the reaction at 5 °C.

chemical mechanism (Scheme 1). In the kinetic/chemical mechanism, addition of O_2 to the TauD·Fe(II)·αKG·taurine complex leads through two nonaccumulating complexes (species **I** and **II**) to **J**. Decay of **J** and taurine hydroxylation by abstraction of an H atom from C1 and radical rebound appears kinetically as a single step and generates the second intermediate, which decays in the rate-limiting step back to the reactant quaternary complex. The second intermediate could be either an enzyme·product(s) complex or the binary TauD·Fe(II) complex awaiting rebinding of substrates. Thus, conversion of the second intermediate state to the O_2-reactive quaternary complex could potentially involve product dissociation, substrate rebinding, a protein conformational change, or some combination of these processes.

The kinetic/chemical mechanism (Scheme 1) makes several predictions. First, formation of **J** should be kinetically first-order with respect to oxygen and the quaternary TauD·Fe(II)·αKG·taurine complex, so long as the intervening intermediates fail to accumulate. Second, release of CO_2 from αKG should occur concomitantly with formation of **J**. Finally, the second intermediate should accumulate to an extent that direct spectroscopic evidence for its existence and nature might be obtained. Importantly, elucidation of the nature of this state would define the rate-limiting step in TauD catalysis, which is conversion of the second intermediate back to the O_2-reactive quaternary complex.

In this study, the above predictions and outstanding questions have been addressed experimentally to evaluate and expand the published description of the TauD reaction cycle. The results are in full accordance with the published kinetic and chemical mechanisms and establish (1) that intermediates between the reactant quaternary complex and **J** accumulate to a minor extent or not at all under these reaction conditions, (2) that decarboxylation of αKG precedes or accompanies formation of **J**, and (3) that the rate-limiting step in the TauD cycle is dissociation of product(s).

MATERIALS AND METHODS

Materials. Culture media components (yeast extract and tryptone) were purchased from Marcor Development Corporation (Hackensack, NJ). Isopropyl-*β*-D-thiogalactopyranoside (IPTG) was purchased from Biosynth International (Naperville, IL). Ampicillin was purchased from IBI (Shelton, CT). 5,5′-Dithio-bis-(2-nitrobenzoic acid) (Ellman's reagent) was purchased from Pierce (Rockford, IL). Glycerol, ammonium sulfate, sodium chloride, ferrous ammonium sulfate, and sodium hydroxide were purchased from EM Science (Gibbstown, NJ). Trizma (Tris) base, 2-aminoethane-1-sulfonic acid (taurine), 2-oxoglutarate (αKG), sodium sulfite, imidazole, poly(ethyleneimine), ethylenediaminetetraacetic acid (EDTA), sodium hydrosulfite (sodium dithionite), and 2-methylbutane were purchased from Sigma Corp. (St. Louis, MO). Trichloroacetic acid and sulfuric acid were purchased from Fisher Scientific (Pittsburgh, PA). Dithiothreitol (DTT) was purchased from United States Biochemical (Cleveland, OH). DEAE-Sepharose FF resin was purchased from Pharmacia (Piscataway, NJ). ^{57}Fe metal was purchased from Advanced Materials and Technologies (New York, NY). 1-[^{14}C]-αKG was purchased from New England Nuclear (Boston, MA). All reagents used for synthesis of 1,1-[^{2}H]$_2$-taurine were purchased from Aldrich Chemical Corp. (St. Louis, MO) and, unless otherwise noted,

Scheme 2: Synthetic Route to 1,1-$[^2H]_2$-taurine

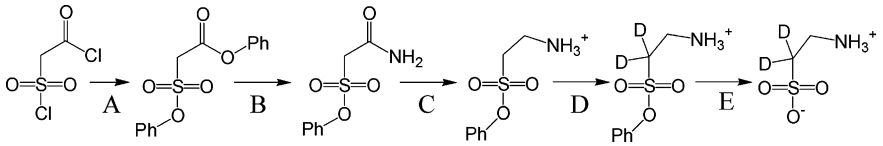

were used without further purification. Silica gel for the column chromatography was purchased from Sorbent Technologies (Atlanta, GA). *O*-$[^2H]$-*tert*-butyl alcohol (99% isotopic enrichment) and $[^2H]_5$-ammonium hydroxide (99% enrichment) were purchased from Cambridge Isotope Laboratories (Andover, MA).

Preparation and Characterization of TauD. TauD was overexpressed and purified as previously described (*14*), with a single modification. During overnight incubation following induction of expression, cultures were shaken at room temperature (21 ± 1 °C) rather than 18 °C. The quality of TauD preparations was assessed as previously described (*14*) by determination of specific enzyme activity and quantity of Fe(II) taken up in O_2-free titrations of the apoenzyme in the presence of αKG and taurine. These titrations were monitored by development of the metal-to-ligand charge-transfer band at 520 nm.

Synthesis of 1,1-$[^2H]_2$-Taurine. Deuterium-substituted taurine was synthesized from chlorosulfonylacetyl chloride according to Scheme 2. Conversion to the phenoxysulfonyl-acetic acid phenyl ester (step A) was accomplished by a procedure similar to that of Hoogenboom et al. (*18*). Starting material (4.0 g, 23 mmol) was added to phenol (4.7 g, 50 mmol) under an argon atmosphere. Toluene (3 mL) was added to the mixture, followed by refluxing for 12 h. The toluene was removed under vacuum, and the product was purified by chromatography on silica. After adsorption of the crude product, the column was flushed with 1 vol of hexane to remove any residual toluene, and the product was eluted with dichloromethane/hexane (60% dichloromethane by volume). After removal of the solvent under vacuum, the product was obtained as a cream-colored solid (5.4 g, 19 mmol). ^1H NMR (22 °C, 300 MHz, $CDCl_3$): 4.37 ppm singlet (2H), 7.15 ppm multiplet (2H), 7.36 ppm multiplet (8H). ^{13}C NMR (22 °C, 75 MHz, $CDCl_3$): 54.4 ppm singlet, 121.5 ppm singlet, 122.6 ppm singlet, 127.2 ppm singlet, 128.3 ppm singlet, 130.1 ppm singlet, 130.6 ppm singlet, 149.7 ppm singlet, 150.5 ppm singlet, 160.7 ppm singlet. MS: $m/z = 293$ (MH^+).

Phenoxysulfonyl-acetic acid phenyl ester was converted to carbamoyl-methanesulfonic acid phenyl ester (Scheme 2, step B) by the procedure of Hoogenboom et al. (*18*). Ammonia (∼ 30 mL) was condensed from the gas phase onto the phenoxysulfonyl-acetic acid phenyl ester (4.0 g, 14 mmol), and the mixture was stirred overnight at −35 °C. Ethanol (∼ 10 mL of 100%) was added to the solution, which was refluxed for 30 min and then adsorbed onto silica. The product was purified by column chromatography using 1:1 (v/v) ethyl acetate/hexane as the mobile phase. After removal of solvent under vacuum, carbamoyl-methanesulfonic acid phenyl ester was obtained as a white solid (2.8 g, 13 mmol). ^1H NMR (22 °C, 300 MHz, $CDCl_3$): 4.2 ppm singlet (2H), 5.8 ppm singlet (1H), 6.6 ppm singlet (1H), 7.4 ppm multiplet (5H). ^{13}C NMR (22 °C, 75 MHz, $CDCl_3$): 55.2 ppm singlet, 122.6 ppm singlet, 128.4 ppm singlet, 130.7 ppm singlet, 149.5 ppm singlet, 161.9 ppm singlet. MS: $m/z = 216$ (MH^+).

Carbamoyl-methanesulfonic acid phenyl ester was reduced to 2-aminoethane-1-sulfonic acid phenyl ester (Scheme 2, step C) using a borane-methyl sulfide complex. Carbamoyl-methanesulfonic acid phenyl ester (2.6 g, 12 mmol) was dissolved under an argon atmosphere in 200 mL of tetrahydrofuran, which had been distilled from sodium and benzophenone. This solution was cooled to 0 °C, and borane-dimethyl sulfide (20 mL, 40 mmol) was dripped in as a 2 M solution in tetrahydrofuran. This solution was then heated to reflux, stirred for 2 h, and allowed to cool. Ethyl acetate (100 mL) was added, and the solution was washed with saturated aqueous solutions of ammonium chloride and then sodium chloride. The organic phase was dried over anhydrous magnesium sulfate and reduced to a clear viscous oil under vacuum. This oil was then stirred in diethylamine a minimum of 4 h, after which the diethylamine was removed under vacuum. The resulting white solid was purified by column chromatography on silica using 2% methanol in dichloromethane as the mobile phase. The product (1.2 g, 6.0 mmol) was collected as a clear oil after removal of solvents under vacuum. ^1H NMR (22 °C, 300 MHz, $CDCl_3$): 1.4 ppm singlet (2H), 3.4 ppm multiplet (4H), 7.3 ppm multiplet (5H). ^{13}C NMR: (22 °C, 75 MHz, $CDCl_3$) 37.4 ppm singlet, 54.1 ppm singlet, 122.5 ppm singlet, 127.8 ppm singlet, 130.4 ppm singlet, 149.5 ppm singlet. MS: $m/z = 202$ (MH^+).

Exchange of the C1 protia of 2-aminoethane-1-sulfonic acid phenyl ester for deuteria was effected by treatment with sodium *t*-butoxide in *O*-$[^2H]$-*tert*-butyl alcohol (Scheme 2, step D). 2-Aminoethane-1-sulfonic acid phenyl ester (0.50 g, 2.5 mmol) was dissolved in 30 mL of *O*-$[^2H]$-*tert*-butyl alcohol (99% isotopic enrichment) under an argon atmosphere. Sodium *t*-butoxide (0.096 g, 1.0 mmol) was added to this solution, which was stirred at 60 °C overnight. ^2H_2O (60 mL, 99.9% isotopic enrichment) was added to quench the exchange reaction. This mixture was extracted with dichloromethane, and the *tert*-butyl alcohol layer was reduced under vacuum to a pale yellow, viscous oil. This material was carried forward without further purification. The contaminant contributing the pale yellow color could be removed by column chromatography on silica gel using 2% methanol in dichloromethane as mobile phase. After removal of the solvent, 1,1-$[^2H]_2$-2-amino-ethanesulfonic acid phenyl ester (0.30 g, 1.5 mmol) was obtained as a clear, viscous oil. ^1H NMR (22 °C, 300 MHz, $CDCl_3$): 1.4 ppm singlet (2H), 3.3 ppm singlet (2H), 7.3 ppm multiplet (5H). ^{13}C NMR (22 °C, 75 MHz, $CDCl_3$): 37.4 ppm singlet, 122.5 ppm singlet, 127.8 ppm singlet, 130.4 ppm singlet, 149.5 ppm singlet. MS: $m/z = 204$ (MH^+).

1,1-$[^2H]_2$-2-aminoethane-1-sulfonic acid phenyl ester was converted to the free acid via hydrogenolysis of the phenolic carbon−oxygen bond (Scheme 2, step E) in a procedure similar to that described by Sturm et al. (*19*). The ester (0.30

g, 1.5 mmol) was dissolved in 12 mL of tetrahydrofuran, which had been distilled from sodium and benzophenone. To this solution was added 1.8 mL of $[^2H]_5$-ammonium hydroxide (26% in ^2H_2O) and 0.15 g 10% palladium on carbon (Pd/C) catalyst. This mixture was then capped and stirred for 3 h under just greater than 1 atm H_2(g). After filtration, the solution was extracted with dichloromethane. Lyophilization of the aqueous layer afforded 1,1-$[^2H]_2$-2-aminoethane-1-sulfonic acid (0.15 g, 1.0 mmol) as a fine white powder. ^{1}H NMR (22 °C, 300 MHz, D_2O): 3.05 ppm triplet (2H), 3.3 ppm triplet (2H). ^{13}C NMR (22 °C, 75 MHz, D_2O): 47.7 ppm singlet, 35.7 ppm singlet. HRMS: m/z = 126.0198 (M−).

Steady-State Rates of CO_2 and Sulfite Production. Assays monitoring $^{14}CO_2$ release from 1-[^{14}C]-αKG and sulfite release from taurine in the steady-state followed the procedures described in our previous work (*15*).

Kinetics of CO_2 Production in a Single Turnover. The kinetics of production of $^{14}CO_2$ from 1-[^{14}C]-αKG in a single turnover were determined by chemical quenched-flow experiments. Oxygen was removed from concentrated stocks of pure TauD in 50 mM Tris·HCl, pH 7.6 (buffer A), as previously described (*14*). In a glovebox (MBraun; Peabody, MA) containing a nitrogen atmosphere, O_2-free solutions of αKG, taurine and ferrous ammonium sulfate were prepared from dry stocks by dissolution in buffer A. Aliquots of these stocks were added to the enzyme to achieve the concentrations listed in the legend to Figure 2. 1-[^{14}C]-αKG, supplied in 10% ethanol in water, was added directly to the protein solution in an aliquot small enough to ensure that the final ethanol concentration was less than 0.02%. The protein solution was centrifuged for 3 min at the maximum speed in an Eppendorf Minispin microcentrifuge and then loaded into one syringe of an Update Instruments System 1000 chemical/freeze-quench apparatus. Air-saturated buffer and the quench solution (either 2 M HCl or 4 M NaOH) were loaded into separate syringes. In the experiment, actuation of the ram drive caused the protein and O_2-saturated buffer to be mixed at 5 °C and to pass through a reaction hose of length appropriate to give the desired reaction time. Upon emerging from the reaction hose, this solution was mixed with the quench solution and then injected into a 15 mL scintillation vial. Within 30 s, a CO_2 trap (a 1 mm square piece of filter paper that had been soaked in 2 M NaOH and then placed in a smaller plastic scintillation vial) was placed inside, the entire system was sealed with a rubber septum, and 1.2 mL 2 M HCl was injected through the septum. The entire system was gently shaken for 90 min at room temperature to allow for trapping of the $^{14}CO_2$. The filter paper was removed and dried overnight at 37 °C in a fresh scintillation vial. An 8 mL aliquot of scintillation fluid was added to each of the two vials containing the original quenched reaction mixture and the dried CO_2 trap. Radioactivity present in each vial was quantified in a Perkin-Elmer 1217 Rackbeta scintillation counter. To account for variation in the volume of sample delivered in the quenched-flow "shots," the radioactivity in the volatile (trap) fraction (corresponding to $^{14}CO_2$) was divided by the sum of the radioactivity in the volatile and nonvolatile (sample) fractions to obtain a fractional conversion.

Stopped-Flow Absorption Experiments and Kinetic Simulations. Stopped-flow absorption experiments were performed at 5 °C on an Applied Photophysics (Surrey, U.K.) SX.18MV stopped-flow apparatus equipped with a photodiode array detector and housed in the MBraun anoxic chamber. In all cases, the optical path length was 1 cm. For the series of experiments examining the dependence of formation of **J** on [O_2], the O_2-free TauD·Fe(II)·αKG·taurine complex was mixed in the stopped-flow apparatus with buffer solutions containing varying [O_2], which were prepared by mixing appropriate volumes of O_2-saturated and O_2-free buffer solutions. The stopped-flow mixing ratio was either 1:1 or 2:5 (protein/O_2-buffer). For experiments investigating binding of substrates, the mixing ratio was 1:1. In some experiments with small absorbance changes, a photomultiplier detector was used in place of the diode array. Experimental details, including final reactant concentrations, are given in the figure legends. Simulation of the stopped-flow kinetic data was accomplished with the program KinTekSim (KinTek Corporation, Austin, TX).

Preparation of Freeze-Quench Mössbauer Samples. Preparation of freeze-quenched samples for Mössbauer analysis was carried out as previously described (*14*). Reactant concentrations and reaction times are given in the appropriate figure legend.

Mössbauer Spectroscopy and Data Analysis. Mössbauer spectra were recorded on a spectrometer from WEB research (Edina, MN) operating in the constant acceleration mode in transmission geometry. Spectra were recorded with the temperature of the sample maintained at 4.2 K. The sample was kept inside an SVT-400 dewar from Janis (Wilmington, MA), and a magnetic field of 40 mT was applied parallel to the γ-beam. The quoted isomer shifts are relative to the centroid of the spectrum of a metallic foil of α-Fe at room temperature. Data deconvolution and analysis were performed by using the program WMOSS from WEB research and the Mathematica software package from Wolfram Research Inc. (Champaign, IL).

RESULTS AND DISCUSSION

*Dependence of the Kinetics of **J** on Concentration of O_2.* In the synthesis of the TauD kinetic and chemical mechanisms presented in Scheme 1, the 318-nm-absorbing **J** forms from the TauD·Fe(II)·αKG·taurine complex and O_2 via two intervening species that, because of unfavorable kinetics (i.e., slower formation and faster decay), do not accumulate. Thus, the scheme predicts that formation of **J** should be kinetically first-order in the quaternary complex and first-order in O_2. The dependence on [O_2] was interrogated specifically, with the quaternary complex as the limiting reactant and a maximum O_2 concentration of 1.4 mM (*20*). As predicted, A_{318}-versus-time traces (Figure 1) show a clear dependence on [O_2] in the formation phase. Values of k_{obs} extracted by fitting the equation for a two-exponential rise−fall to these data show a linear dependence on [O_2] (inset to Figure 1A). To evaluate the concentration dependence more rigorously (without complication from the incomplete kinetic resolution of the formation and decay phases and the violation of pseudo-first-order conditions at low [O_2]), traces were simulated (solid lines in Figure 1A) according to the published 3-step kinetic mechanism (*14*). Agreement is good after the first ∼15 ms. The deviation at shorter reaction times may be a result of a prolonged mixing artifact. Indeed, the

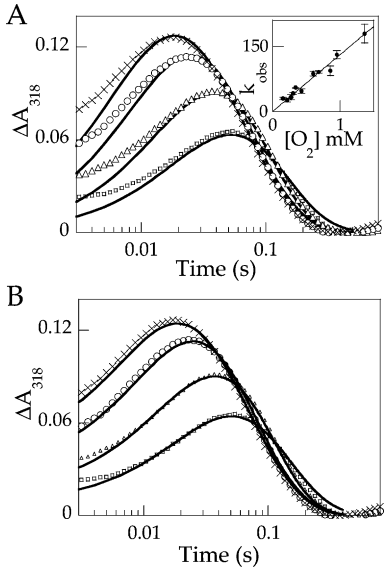

FIGURE 1: Absorbance-versus-time traces (318 nm) after mixing at 5 °C of an O_2-free solution containing 0.72 mM TauD, 0.5 mM Fe(II), 0.1 mM αKG, and 4.28 mM taurine in buffer A with an equal volume of buffer A containing varying concentrations of O_2. The symbols are the data from experiments with final O_2 concentrations of 0.15 mM (squares), 0.3 mM (triangles), 0.6 mM (circles), and 0.95 mM (crosses). The solid lines are from simulations that are described in the text and that employed the parameters shown in Table S1 (Supporting Information). (A) Simulations according to the three-step minimal kinetic mechanism (*14*). (B) Simulations based on a four-step mechanism that includes a dissociable initial O_2 complex as a precursor to **J**.

first few milliseconds of data show a steep decay phase that is certainly a mixing artifact. If this artifact is not fully extinguished until ∼15 ms, then the deviation of the experimental traces from the theoretical traces would be explained. Alternatively, the deviation at early time could reflect accumulation of an absorbing precursor to **J**. Indeed, the resonance Raman study of Proshlyakov et al. reported a band at 583 cm^{-1} that shifted to 555 cm^{-1} when the reaction was carried out with $^{18}O_2$ (*16*). This feature was tentatively ascribed to an additional intermediate, possibly a precursor to **J**. To assess the possibility that a precursor accumulates, the A_{318} traces were simulated according to an expanded kinetic mechanism that includes a dissociable initial complex with O_2 as a precursor to **J** (lines in Figure 1B; parameter values are given in Figure S1, Supporting Information). The expanded mechanism allows for better agreement in the early regions of the traces due to absorbance from the precursor. However, the approximately first-order dependence of the traces on $[O_2]$ at longer times effectively sets upper limits both on the quantity of the precursor that can accumulate (∼0.3 equiv) and on the time of maximal accumulation (∼1 ms). The minimal and fast accumulation of such a species would explain its failure to be detected in previous freeze-quench Mössbauer experiments, in which a quench time of 10 ms was estimated and **J** was observed to have reached or approached its maximum level at the shortest accessible reaction time. Faster quenching (*21*) or lower reaction temperatures (*16*) would be required for detection of such a species by freeze-quench Mössbauer.

While this work was in review, Grzyska et al. (*22*) published the results of similar experiments examining the dependence of the kinetics of **J** on $[O_2]$. Over a smaller range of $[O_2]$ (<0.6 mM compared to <1.4 mM in the present study), these authors also demonstrated (by the same analysis depicted in the inset to Figure 1A) an approximately first-order dependence. In this case, simulations of individual traces were not shown, and no attempt was made to set an upper limit for accumulation of a precursor to **J**.

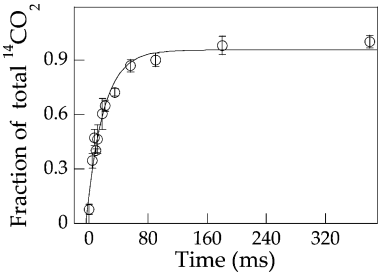

FIGURE 2: Kinetics of production of $^{14}CO_2$ from 1-[^{14}C]-αKG in single-turnover, chemical-quenched-flow experiments in which the TauD·Fe(II)·αKG·taurine complex in buffer A was mixed at 5 °C with O_2-containing buffer A. The concentrations after mixing were 1.1 mM TauD, 1 mM Fe(II), 0.06 mM αKG, and 5 mM taurine. The circular points are average values from experiments using either 4 N NaOH or 2 N H_2SO_4 as the quench solution. The error bars are the standard deviations for each reaction time in five independent trials. The solid line is a fit of the equation for an exponential increase and corresponds to $k = 42\ s^{-1}$. From this value and the O_2 concentration of 0.26 mM, a second-order rate constant of $1.6 \times 10^5\ M^{-1}\ s^{-1}$ is calculated.

Kinetics of Decarboxylation of αKG in a Single Turnover. To assess the timing of decarboxylation of αKG relative to formation of **J** and, thus, to determine whether the C1 carboxylate ligand is present in the intermediate, the kinetics of $^{14}CO_2$ production in a single turnover were defined in chemical quenched-flow experiments with 1-[^{14}C]-αKG. Given the K_D for αKG binding of the TauD·Fe(II) complex in the presence of 5 mM taurine (20 ± 19 μM) (*23*), the concentration of protein (1 mM) was sufficiently high to ensure that the αKG was 98% saturated with enzyme. Acid, base, and denaturant quenching were tested. Acid and base quenching yielded kinetic data in mutual agreement, and fitting the compiled data as an exponential rise gave an apparent first-order rate constant of 42 s^{-1} (Figure 2). With the concentration of O_2 employed (0.26 mM), this apparent first-order rate constant corresponds to a second-order rate constant of $1.6 \times 10^5\ M^{-1}\ s^{-1}$, in excellent agreement with the value obtained in simulation of the stopped-flow absorption data ($(1.5 \pm 0.2) \times 10^5\ M^{-1}\ s^{-1}$). These results suggest that decarboxylation occurs during formation of **J**. To assess the less likely possibility that decarboxylation occurs *after* formation of **J** but both acid and base quenching lead to cleavage of the intact C1−C2 bond in this complex, attempts were made to quench with organic solvents (THF) and denaturants (5.5 M urea, 4 M guanidinium·HCl). Unfortunately, none of these treatments terminated the reaction sufficiently rapidly to permit accurate kinetics of $^{14}CO_2$ production to be obtained. Thus, the possibility that both acid and base quenching of **J** induce cleavage of the αKG C1−C2 bond cannot rigorously be excluded.

Nature of the Rate-Limiting Step: Kinetics of Binding of Substrates. As noted, the rate-limiting conversion of the second intermediate back to the reactive quaternary complex could involve substrate binding, product release, a protein conformational change, or some combination of these events. A previous study (*23*) reported that binding of αKG to the

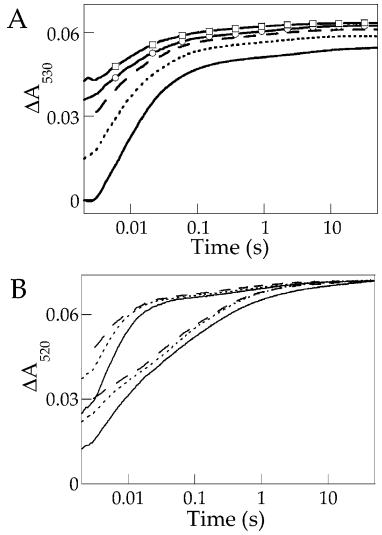

FIGURE 3: Absorbance-versus-time traces monitoring binding of αKG in the absence (A) and presence (B) of taurine. In A, TauD containing 0.69 equiv of Fe(II) was mixed at 5 °C in the absence of O_2 with solutions of αKG to give final concentrations of 0.49 mM TauD and 1.5 mM (solid trace), 3 mM (dotted trace), 6 mM (dashed trace), 9 mM (solid trace with open circles), or 15 mM (solid trace with open squares) αKG. In B, both sets of traces are from experiments in which TauD containing 0.69 equiv of Fe(II) was mixed with a solution of αKG to give final concentrations of 0.49 mM TauD and 3 mM (solid traces), 6 mM (dotted traces), or 9 mM (dashed traces) αKG. For the lower three traces, taurine was present in the TauD·Fe(II) solution such that [taurine] was 5 mM after mixing. In the upper three traces, taurine was present in the αKG solution, also giving 5 mM taurine after mixing.

binary TauD·Fe(II) complex exhibits zero-order kinetics with respect to αKG and has a rate constant at 4 °C (2−6 s^{-1}) very similar to that reported for conversion of the second intermediate to the reactive quaternary complex at 5 °C (2.5 ± 0.5 s^{-1} (*14*)). Thus, binding of αKG was initially favored as the most likely candidate for the rate-limiting step (*14*). To evaluate this hypothesis, the kinetics of binding of αKG to the TauD·Fe(II) complex in the presence and absence of taurine were examined by monitoring development of the Fe(II)-to-αKG charge-transfer transition at 520−530 nm. Binding of αKG is multiphasic (Figure 3A). With increasing [αKG], the fraction of the reaction that is complete in the dead-time of the instrument (1.3 ms) increases. The shape and λ_{max} of the spectrum that develops in this fastest phase are indistinguishable from those characterizing subsequent changes. A phase with an apparent first-order rate-constant of >100 s^{-1} and observed amplitude that decreases with increasing [αKG] is then observed. A second observed phase with smaller amplitude and an apparent first-order rate constant >20 s^{-1} is observed. Finally, a phase that is too slow to be on the catalytic pathway (k < 0.5 s^{-1}) is also observed at all concentrations. The observation of several kinetic phases may be explained one of two ways. Multiple conformational states of the enzyme may be present, as has previously been proposed (*23, 24*), and these may bind αKG with different kinetics, affinities, or both; alternatively, productive binding of αKG may involve multiple steps, including the bimolecular association of the substrate and enzyme and one or more unimolecular (conformational) steps to convert this initial complex into the species that is competent to go forward in the catalytic cycle. This issue is resolved below. The order of substrate binding was probed

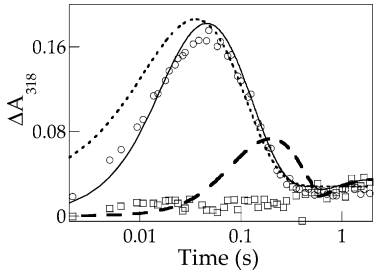

FIGURE 4: Absorbance-versus-time traces after mixing at 5 °C of TauD·Fe(II) complex with O_2, αKG and taurine. Final concentrations after mixing were 0.5 mM TauD·Fe(II), 0.2 mM O_2, 5 mM αKG, and either 0 mM taurine (squares) or 5 mM taurine (circles). The dotted line is a simulation according to the 3-step kinetic mechanism (*14*), which assumes preformed reactive quaternary complex. The dashed line is a simulation according to an expanded mechanism that places a 3 s^{-1} step for quaternary complex formation prior to O_2 addition. The solid line is a simulation according to this same expanded mechanism, but with an effective rate constant of 150 s^{-1} for formation of the quaternary complex.

by additional O_2-free substrate-mixing experiments. Mixing of the TauD·Fe(II)·αKG ternary complex with taurine revealed that the slight shift in λ_{max} of the Fe(II)-to-αKG transition (from 530 to 520 nm) associated with taurine binding (*23*) is complete in the dead-time of the stopped-flow, consistent with the previous report that taurine can bind rapidly after αKG. Mixing of the TauD·Fe(II) complex with both substrates simultaneously gave multiphasic kinetics (Figure 3B, upper three traces) similar to those observed in the mix of the binary complex with αKG alone. The dependence of the absorbance at completion on [αKG] in the absence of taurine (Figure 3A) but independence in its presence (Figure 3B) is a reflection of the previously demonstrated synergistic binding of the two substrates, which reduces the apparent K_D for αKG from ∼300 μM in the absence of taurine to ∼20 μM in the presence of 5 mM taurine (*23*). When taurine was present with the TauD·Fe(II) complex prior to mixing with αKG in the stopped-flow apparatus, development of the chromophore was significantly slowed (Figure 3B, lower three traces). The demonstration by X-ray crystallography that TauD assumes a "closed" conformation upon binding of taurine to the TauD·Fe(II) complex (*24*) provides a simple structural explanation for this observation. The observations that taurine binding to the TauD·Fe(II)·αKG complex is very fast and that prior binding of taurine impedes binding of αKG imply a preferred or obligatory order of substrate binding (αKG and then taurine), as has been observed for other α-ketoacid-dependent dioxygenases (see ref *11* and references therein).

To distinguish whether the kinetic complexity in αKG binding arises from the presence of multiple conformational states (parallel binding processes) or from a multistep (sequential) binding process, an experiment was performed in which the binary TauD·Fe(II) complex was mixed simultaneously with αKG, taurine, and O_2, and the kinetics of formation of **J** were defined by monitoring development of its absorption feature at 318 nm. As shown in Figure 4, formation of **J** is only slightly slower in this reaction than in mixing of the preformed quaternary complex with O_2 (compare circles to dotted trace, which is a simulation for the reaction of preformed quaternary complex with O_2). Results of a control experiment in which taurine was omitted (Figure 4, squares) establish that both substrates must bind

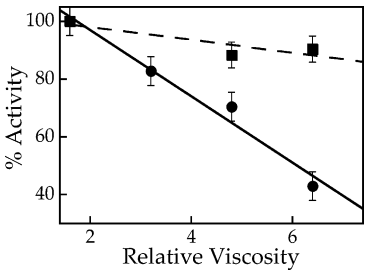

FIGURE 5: Effect of solvent viscosity on the steady-state rates of hydroxylation of 1,1-[^{1}H]$_2$-taurine (circles) and 1,1-[^{2}H]$_2$-taurine (squares). Activity was measured at 5 °C in buffer A with 5 μM TauD, 1 mM Fe(II), 1 mM αKG, 0.5 mM taurine, and ambient O_2 (~380 μM). Glycerol was used to vary the relative viscosity (RV) from 1.6 (0% w/w glycerol) to 6.4 (38% w/w glycerol) (*28*).

for rapid O_2 activation, as has previously been documented in different experiments (*14*). Simulation of the experimental trace implies that the requirement for αKG and taurine binding imposes a lag in formation of **J** characterized by a rate constant of at least 150 s^{-1} (solid trace), corresponding to a second-order rate constant of at least 3×10^4 M^{-1} s^{-1}. By contrast, if a step involved in formation of the O_2-reactive complex were to be primarily rate-limiting (2.5 s^{-1}), formation of **J** would be markedly slower and its accumulation suppressed upon initiation of the reaction by mixing simultaneously with all three substrates (Figure 4, dashed trace). These observations suggest that the kinetic complexity in αKG binding arises from parallel processes involving different states of the enzyme. More importantly, they eliminate substrate binding steps as candidates for the rate-limiting step.

Nature of the Rate-Limiting Step: Solvent Viscosity Effects. The large C1 deuterium kinetic isotope effect ($k_H/k_D \sim 35$) on decay of **J** (*15*) and the absence of accumulation of an Fe complex between **J** and the second intermediate establish that taurine hydroxylation and decay of **J** are kinetically correlated (with a rate constant of 13 ± 2 s^{-1}) and, therefore, that chemical steps also are not rate-limiting. Thus, only steps involved in the release of products remain as viable candidates. Release of products could involve simple dissociation, a protein conformational change required for dissociation, an Fe-ligand-substitution step required for dissociation of a coordinated product (e.g., succinate, as shown in Scheme 1), or some combination of these processes. Variation of solvent viscosity has been used extensively to provide evidence that product release is rate-limiting in enzyme reactions (*25*−*27*). The idea is that diffusion of products away from the active site is less rapid at higher viscosity, leading to diminution of k_{cat} when product dissociation is rate-limiting but not when chemical steps are rate-limiting. Of the possible constituents of product release in the TauD reaction, simple dissociation is expected to be most sensitive (directly proportional) to the relative solvent viscosity (RV). Ligand substitution within the active site should be insensitive, and a conformational change might or might not be slower at higher RV. The dependence of k_{cat} on solvent viscosity was examined, with glycerol used as viscogen, to determine whether the rate-limiting step is diffusional in nature. Indeed, the k_{cat} decreases with increasing solvent viscosity (Figure 5, circular points and solid line). A control experiment was performed with 1,1-[^{2}H]$_2$-taurine as substrate. Previous results have shown that the large deuterium kinetic isotope effect on hydroxylation renders the chemical step rate-limiting for this substrate, which, in turn, should eliminate the solvent viscosity effect. As expected, the dependence of k_{cat} for hydroxylation of 1,1-[^{2}H]$_2$-taurine on RV (Figure 5, square points and dashed line) is much less pronounced (<20% of the effect for 1,1-[^{1}H]$_2$-taurine). These data support the deduction that steps involved in product release limit k_{cat} for hydroxylation of 1,1-[^{1}H]$_2$-taurine. However, because the k_{cat} is not strictly proportional to RV, it is likely that the product release step is complex, involving both simple dissociation and one or more additional steps that are insensitive (or less sensitive) to RV (e.g., ligand dissociation or a conformational change).

Explanation for Previously Observed Slow Phase of TauD·Fe(II)·αKG Complex Regeneration. In the study that first detected **J** and presented the minimal kinetic mechanism for TauD catalysis (*14*), the one aspect of the kinetic data that was not successfully rationalized was a slow phase in regeneration of the 520 nm charge-transfer band of the TauD·Fe(II)·αKG·taurine complex following depletion of O_2 (which was limiting with respect to the other substrates) and decay of the putative Fe(II)-containing intermediate. This phase was too slow to be on the catalytic pathway, implying that it must be attributable to conditions employed in the stopped-flow experiments but not the steady-state determinations of k_{cat} (e.g., the much greater concentration of enzyme). Accumulation of products was cited as a likely cause. The evidence for a preferred or obligatory binding order of αKG and then taurine would suggest that product release probably occurs in the order of 1-hydroxytaurine followed by succinate. Interference with this sequence upon trapping of the TauD·Fe(II)·succinate complex by taurine (which was present in excess in the stopped-flow experiments) might then explain the previously observed slow phase in regeneration of the quaternary complex. This hypothesis makes two predictions that were tested in this study. First, the slow phase should become less pronounced with diminishing concentration of taurine. Figure 6A shows that this prediction is borne out. Second, taurine might become inhibitory at high concentrations. Indeed, taurine inhibition is observed and is most pronounced at higher solvent viscosity (Figure 6B), when release of product (presumably succinate) is retarded (vide supra). Thus, inhibition of succinate release by the out-of-sequence binding of taurine is at least partly responsible for the slow phase of quaternary complex regeneration.

Mössbauer Spectroscopic Evidence for the Fe(II)-Containing Intermediate. Previous evidence for the accumulation of the proposed Fe(II)-containing intermediate was indirect: decay of the 318-nm absorption and Mössbauer quadrupole doublet of **J** were found to occur concomitantly with a regain in intensity of the broad doublet characteristic of high-spin Fe(II) species but prior to regeneration of the 520-nm band of the reactant quaternary complex. These observations required the accumulation of a third state (in addition to the quaternary complex and **J**) and implied that this state contains high-spin Fe(II). To determine if the Mössbauer-spectroscopic features of the inferred second intermediate are distinct from those of the quaternary complex, the spectrum of the previously reported 200-ms sample (*14*) (Figure 7A, hash marks) was reanalyzed. Scheme 1 predicts maximum accumulation of the second intermediate at this time under the reaction conditions employed. The solid line plotted over

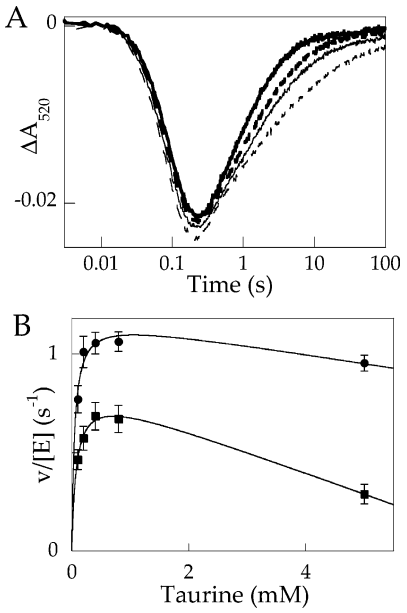

FIGURE 6: Inhibition of (A) regeneration of the quaternary TauD·Fe(II)·αKG·taurine complex after a single turnover and (B) catalysis in the steady state by increasing concentrations of taurine. (A) ΔA_{520}-versus-time traces after mixing at 5 °C of a solution containing 1.2 mM TauD, 1 mM Fe(II), 10 mM αKG, and 2 mM (solid, bold), 6 mM (dashed, bold), 10 mM (solid), or 40 mM taurine (dashed) with an equal volume of air-saturated buffer A. (B) Inhibition of steady-state turnover at 5 °C by high concentrations of taurine at RV = 1.6 (circles) and RV = 4.8 (squares). The assay conditions were the same as in Figure 4, except that the taurine concentration was varied as indicated.

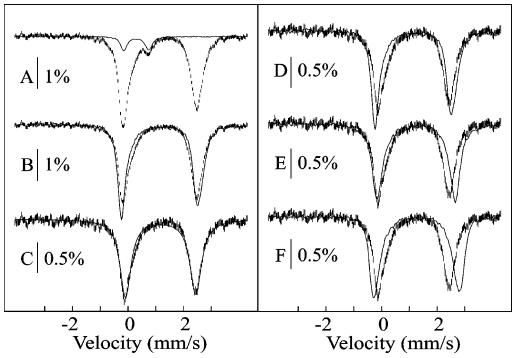

FIGURE 7: Analysis to determine the Mössbauer spectrum of the Fe(II)-containing intermediate (A−C) and comparison to the spectra of the TauD·Fe(II)·αKG·taurine, TauD·Fe(II)·αKG, and TauD·Fe(II) complexes (D−F, respectively). (A) The spectrum of a sample prepared by reacting the TauD·Fe(II)·αKG·taurine complex with O_2 at 5 °C for 200 ms (hash marks). Concentrations after mixing were 1.5 mM TauD, 1.5 mM ^{57}Fe, 5 mM αKG, 5 mM taurine, and 1.3 mM O_2. The solid line is a reference spectrum of **J**, scaled to 11% of the total absorption. (B) Removal of the contribution of **J** to the spectrum in A results in the hash-marked spectrum. The solid line is the spectrum of the TauD·Fe(II)·αKG·taurine complex, scaled to the same intensity. (C) Removal of 35% of the spectrum of the TauD·Fe(II)·αKG·taurine complex results in the reference spectrum for the second intermediate, displayed as hash marks. The solid line overlaid is a quadrupole doublet with the parameters given in the text and Table S1 (Supporting Information). (D−F) The hash-marked spectrum in each case is the reference spectrum of the second intermediate. The solid line is the spectrum of the TauD·Fe(II)·αKG·taurine complex (D), the TauD·Fe(II)·αKG complex (E), or the TauD·Fe(II) complex (F) scaled to the same intensity. All experimental spectra were collected at 4.2 K in a 40-mT magnetic field.

the data is an experimental reference spectrum of **J** (see Figure S2, Supporting Information), scaled to 11% of the total intensity of the spectrum. Removal of the contribution of **J** gives a spectrum (hash marks in Figure 7B) that, although it overlaps considerably with that of the TauD·Fe(II)·αKG·taurine quaternary complex, has an overall splitting of the two peaks that is ∼0.2 mm/s smaller. This result suggests that the spectrum of the second intermediate is partially resolved from that of the reactant complex due primarily to a smaller quadrupole splitting parameter, ΔE_Q. To generate a reference spectrum of the second intermediate, the contribution arising from the quaternary complex must be removed. Whereas it is not possible to determine the quantity of quaternary complex present in the 200-ms sample from analysis of the Mössbauer spectrum, this value can be estimated based on the following considerations. Previous analysis of data from this experiment (*14*) had revealed that only 70% of the TauD·Fe(II)·αKG·taurine complex reacted rapidly with oxygen, whereas the remaining 30% did not react (or reacted much less rapidly). In addition to the 30% of inactive quaternary complex, Scheme 1 predicts 8% of the catalytically active Fe sites to have re-formed the quaternary complex after 200 ms, thus allowing us to estimate that the 200-ms sample contains 35% quaternary complex (30% inactive and 8% of 70% catalytically active). The reference spectrum of the second intermediate (Figure 7C, hashed marks) is thus obtained by subtracting 35% of the spectrum of the quaternary complex from the spectrum of Figure 7B. Fitting the resulting spectrum as one quadrupole doublet (Figure 7C, solid line) yields $\delta = 1.17$ mm/s and $\Delta E_Q = 2.56$ for the second intermediate. As a measure of the uncertainty in these parameters, several additional reference spectra of the second intermediate were generated by removing varying contributions from the quaternary complex (25−45% in 5% increments). These reference spectra were then fitted by a single quadrupole doublet. Under this analysis, the isomer shift varies from 1.17 to 1.18 mm/s and that the quadrupole splitting parameter varies from 2.52 to 2.59 mm/s (Table S1, Supporting Information). The uncertainty of ΔE_Q is caused by the overlapping nature of the spectral features of the quaternary complex and the second intermediate; when less quaternary complex is removed, the ΔE_Q deduced for the second intermediate is larger, because the quaternary complex has a larger ΔE_Q.

Whereas it is not possible to determine whether the features that we attribute to the second intermediate arise from one species or several species with similar Mössbauer parameters, it is clear that they are distinct from those of the quaternary complex. Moreover, these features are distinct from those of the binary TauD·Fe(II) and ternary TauD·Fe(II)·αKG complexes, because the high-energy lines of these complexes are at even higher energies (2.78 and 2.65 mm/s, respectively) than that of the quaternary complex. This is illustrated in Figure 7D−F, in which the reference spectrum of the second intermediate (hash marks) is compared to spectra of the quaternary, ternary, and binary complexes, respectively (solid lines).

To determine the kinetics of the second intermediate by Mössbauer spectroscopy, the time-dependent spectra were analyzed under the assumption that each spectrum can be described as a superposition of three reference spectra, representing the quaternary complex, **J**, and the second intermediate. Fitting of the experimental data was performed

Table 1: Relative Amounts, Given as a Percentage of the Total Iron Concentration, of TauD·Fe(II)·αKG·Taurine, **J**, and the Second Intermediate, Determined by Mössbauer Spectroscopy

time (s)	TauD·Fe(II)·αKG·taurine	**J**	Fe(II) intermediate
	Formation Time Course		
0.02	48 ± 3	44 ± 3	8 ± 3
0.08	29 ± 6	26 ± 3	42 ± 6
0.2	35 ± 10	11 ± 3	54 ± 10
	Decay Time Course		
0.02	43 ± 3	48 ± 3	9 ± 3
0.42	53 ± 8	5 ± 3	42 ± 8
1	59 ± 6	<3	38 ± 6
3	65 ± 5	<3	32 ± 5
6	69 ± 4	<3	28 ± 4
8	74 ± 4	<3	23 ± 4
10	73 ± 4	<3	24 ± 4

by systematically sampling linear combinations of the reference spectra, with coefficients varied in step sizes of 1% of the total absorption. The linear combination with the lowest χ^2-value was considered to be the best solution. The relative amount of each component was then calculated by the relative area contributed by its reference spectrum. This correlation relies on the justified assumption that the Mössbauer *f*-factor is the same for all species at 4.2 K. This analysis was carried out for the set of five reference spectra for the second intermediate described above.

Two series of samples (time courses) were analyzed. The first time course previously reported in Price et al. (*14*) was reanalyzed to determine the kinetics of formation of the second intermediate. A new time course was prepared to define the kinetics of decay of the second intermediate and the reappearance of the quaternary complex. For this new time course, simulation of the kinetics of **J** confirmed that, as in the previously described experiment, only ~70% of the Fe(II) present in the sample was competent to react rapidly with O_2 to form **J**. The results of the analyses of the two time courses are summarized in Table 1. The experimental Mössbauer spectrum for each time point of the decay time course (hash marks) and the best fit to the experimental spectrum (solid line), which corresponds to the summation of reference spectra in the proportions given in Table 1, are shown in Figure S3, Supporting Information. The range of the relative amounts of the three species was obtained from the analysis with the five sets of reference spectra. The large uncertainties observed for the quantities of the quaternary complex and second intermediate are caused by the significant overlap of their spectral features. To test whether the deconvolutions of the Mössbauer are meaningful, these results were compared to those obtained independently from stopped-flow absorption experiments. Because the regeneration of the quaternary complex as monitored by the increase of absorption at 520 nm in stopped-flow absorption experiments is not well-reproduced by simulations using the simple three-state model, the kinetic data from the Mössbauer analyses were compared directly to stopped-flow data from an experiment with similar reaction conditions (see Figure 8). At 480 nm, the reactant quaternary complex and **J** are approximately isosbestic. Thus, the decay and rebound of absorbance at this wavelength should correlate with the accumulation and disappearance, respectively, of the less intensely absorbing second intermediate. At 600 nm, **J** and the second intermediate are essentially transparent, and thus,

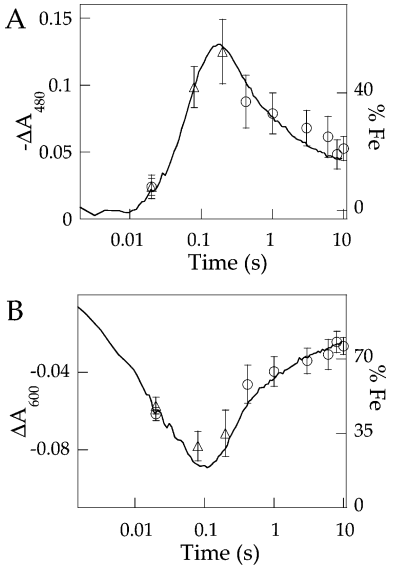

FIGURE 8: Time dependence of the relative amounts of the second intermediate (A) and the TauD·Fe(II)·αKG·taurine complex (B) obtained from analysis of stopped-flow absorption (left axis) and Mössbauer (right axis) spectroscopic experiments. The negative of the absorbance changes monitored at 480 nm ($-\Delta A_{480}$, solid line in panel A) correlates with the concentration of the second intermediate. The absorbance change at 600 nm (A_{600}, solid line in panel B) correlates with the concentration of the TauD·Fe(II)·αKG·taurine complex. Relative amounts obtained from analysis of the Mössbauer data are shown as circles (decay time course) and triangles (formation time course) in panels A and B. The error bars reflect the results obtained from analyses using reference spectra for the second intermediate, which were generated by removing either more (45%) or less (25%) of the quaternary complex than its estimated amount (35%). For both plots, the scales were determined as described in the text. The final concentrations in the stopped-flow experiment were 2 mM TauD, 1.4 mM Fe(II), 5 mM αKG, 5 mM taurine, and 0.9 mM O_2, and those in the Mössbauer experiment are given in the legend of Figure S3 (Supporting Information).

the A_{600}-versus-time trace should directly reflect disappearance and reaccumulation of the quaternary complex. Previous work allows estimation of the extinction coefficients for all three species at both wavelengths: $\epsilon_{480} = 185\ M^{-1}cm^{-1}$ and $\epsilon_{600} = 130\ M^{-1}cm^{-1}$ for the quaternary complex, $\epsilon_{480} = 185\ M^{-1}cm^{-1}$ and $\epsilon_{600} = 0\ M^{-1}cm^{-1}$ for **J**, and $\epsilon_{480} = 0\ M^{-1}cm^{-1}$ and $\epsilon_{600} = 0\ M^{-1}cm^{-1}$ for the second intermediate. The concentrations of the species can be obtained from Mössbauer by correlating the relative amounts with the known total ^{57}Fe concentration. Comparison of these concentrations to the stopped-flow absorption kinetic data scaled according to the estimated molar absorptivities is shown in Figure 8 for the second intermediate (panel A) and the quaternary complex (panel B). The agreement is satisfactory and corroborates that the partially resolved Mössbauer features do, in fact, arise from the second intermediate.

Attempts to generate a species with this same partially resolved Mössbauer spectrum by addition of succinate to the TauD·Fe(II) binary complex, either in the presence or absence of taurine, were unsuccessful. Whereas perturbations to the spectrum were observed, the resulting features were broad and did not reproduce those deduced for the second intermediate. It is likely that the product state differs in some important aspect as a result of having been formed through the catalytic cycle. For example, the Fe(II) may have a low coordination number (as depicted in Scheme 1) that is not

reproduced merely by binding of succinate to the (presumably initially six-coordinate) Fe(II) of the resting binary complex.

ACKNOWLEDGMENT

We thank Dr. Timothy E. Glass and John C. Hanley for their valuable advice and the use of their facilities during the development of the synthetic procedure for 1,1-$[^2H]_2$-taurine.

SUPPORTING INFORMATION AVAILABLE

Parameters used for the simulation of oxygen dependence of the stopped-flow absorption data, a table with Mössbauer parameters of the second intermediate, a figure of the reference spectrum of **J**, and a figure of the spectra for the individual freeze-quench time points. This material is available free of charge via the Internet at http://pubs.acs.org.

REFERENCES

1. Hausinger, R. P. (2004) Fe(II)/α-ketoglutarate-dependent hydroxylases and related enzymes, *Crit. Rev. Biochem. Mol. Biol. 39*, 21−68.
2. Myllyharju, J. (2003) Prolyl 4-hydroxylases, the key enzymes of collagen biosynthesis, *Matrix Biol. 22*, 15−24.
3. Ivan, M., Kondo, K., Yang, H., Kim, W., Valiando, J., Ohh, M., Salic, A., Asara, J. M., Lane, W. S., and Kaelin, W. G., Jr. (2001) HIFα targeted for VHL-mediated destruction by proline hydroxylation: implications for O_2 sensing, *Science 292*, 464−468.
4. Jaakkola, P., Mole, D. R., Tian, Y.-M., Wilson, M. I., Gielbert, J., Gaskell, S. J., von Kriegsheim, A., Hebestreit, H. F., Mukherji, M., Schofield, C. J., Maxwell, P. H., Pugh, C. W., and Ratcliffe, P. J. (2001) Targeting of HIFα to the von Hippel-Lindau ubiquitylation complex by O_2-regulated prolyl hydroxylation, *Science 292*, 468−472.
5. Choroba, O. W., Williams, D. H., and Spencer, J. B. (2000) Biosynthesis of the vancomycin group of antibiotics: involvement of an unusual dioxygenase in the pathway to (*S*)-4-hydroxyphenylglycine, *J. Am. Chem. Soc. 122*, 5389−5390.
6. Baldwin, J. E., Adlington, R. M., Crouch, N. P., Schofield, C. J., Turner, N. J., and Aplin, R. T. (1991) Cephalosporin biosynthesis: a branched pathway sensitive to an isotope effect, *Tetrahedron 47*, 9881−9900.
7. Baldwin, J. E., and Bradley, M. (1990) Isopenicillin N synthase: mechanistic studies, *Chem. Rev. 90*, 1079−1088.
8. Duncan, T., Trewick, S. C., Koivisto, P., Bates, P. A., Lindahl, T., and Sedgwick, B. (2002) Reversal of DNA alkylation damage by two human dioxygenases, *Proc. Natl. Acad. Sci. U.S.A. 99*, 16660−16665.
9. Trewick, S. C., Henshaw, T. F., Hausinger, R. P., Lindahl, T., and Sedgwick, B. (2002) Oxidative demethylation by *Escherichia coli* AlkB directly reverts DNA base damage, *Nature 419*, 174−178.
10. Eichhorn, E., van der Ploeg, J. R., Kertesz, M. A., and Leisinger, T. (1997) Characterization of α-ketoglutarate-dependent taurine dioxygenase from *Escherichia coli*, *J. Biol. Chem. 272*, 23031−23036.
11. Costas, M., Mehn, M. P., Jensen, M. P., and Que, L., Jr. (2004) Dioxygen activation at mononuclear nonheme iron active sites: enzymes, models, and intermediates, *Chem. Rev. 104*, 939−986.
12. Solomon, E. I., Brunold, T. C., Davis, M. I., Kemsley, J. N., Lee, S. K., Lehnert, N., Neese, F., Skulan, A. J., Yang, Y.-S., and Zhou, J. (2000) Geometric and electronic structure/function correlations in non-heme iron enzymes, *Chem. Rev. 100*, 235−349.
13. Hanauske-Abel, H. M., and Günzler, V. (1982) A stereochemical concept for the catalytic mechanism of prolylhydroxylase. Applicability to classification and design of inhibitors, *J. Theor. Biol. 94*, 421−455.
14. Price, J. C., Barr, E. W., Tirupati, B., Bollinger, J. M., Jr., and Krebs, C. (2003) The first direct characterization of a high-valent iron intermediate in the reaction of an α-ketoglutarate-dependent dioxygenase: a high-spin Fe(IV) complex in taurine/α-ketoglutarate dioxygenase (TauD) from *Escherichia coli*, *Biochemistry 42*, 7497−7508.
15. Price, J. C., Barr, E. W., Glass, T. E., Krebs, C., and Bollinger, J. M., Jr. (2003) Evidence for hydrogen abstraction from C1 of taurine by the high-spin Fe(IV) intermediate detected during oxygen activation by taurine:α-ketoglutarate dioxygenase (TauD), *J. Am. Chem. Soc. 125*, 13008−13009.
16. Proshlyakov, D. A., Henshaw, T. F., Monterosso, G. R., Ryle, M. J., and Hausinger, R. P. (2004) Direct detection of oxygen intermediates in the non-heme Fe enzyme taurine/α-ketoglutarate dioxygenase, *J. Am. Chem. Soc. 126*, 1022−1023.
17. Riggs-Gelasco, P. J., Price, J. C., Guyer, R. B., Brehm, J. H., Barr, E. W., Bollinger, J. M., Jr., and Krebs, C. (2004) EXAFS spectroscopic evidence for an Fe═O unit in the Fe(IV) intermediate observed during oxygen activation by taurine:α-ketoglutarate dioxygenase, *J. Am. Chem. Soc. 126*, 8108−8109.
18. Hoogenboom, B. E., Abbott, R., Locatell, L., Jr., and Hinman, R. L. (1959) Chemistry of the 1,2,4-thiadiazine ring system. II. New synthesis of 1,2,4,*2H*-thiadiazine-3,5(*4H*,*6H*)-dione 1,1-dioxide, *J. Org. Chem. 24*, 1983−1986.
19. Sturm, K., Muschaweck, R., and Hropot, M. (1983) 5-Sulfamoylorthanilic acids, a sulfonamide series with salidiuretic activity, *J. Med. Chem. 26*, 1174−1187.
20. Hitchman, M. L. (1978) *Chemical Analysis, Vol. 49: Measurement of Dissolved Oxygen*, Wiley, New York.
21. Cherepanov, A. V., and de Vries, S. (2004) Microsecond freeze-hyperquenching: development of a new ultrafast micro-mixing and sampling technology and application to enzyme catalysis, *Biochem. Biophys. Acta 1656*, 1−31.
22. Grzyska, P. K., Ryle, M. J., Monterosso, G. R., Liu, J., Ballou, D. P., and Hausinger, R. P. (2005) Steady-state and transient kinetic analyses of taurine/α-ketoglutarate dioxygenase: effects of oxygen concentration, alternative sulfonates, and active-site variants on the Fe(IV)-oxo intermediate, *Biochemistry 44*, 3845−3855.
23. Ryle, M. J., Padmakumar, R., and Hausinger, R. P. (1999) Stopped-flow kinetic analysis of *Escherichia coli* taurine/α-ketoglutarate dioxygenase: interactions with α-ketoglutarate, taurine, and oxygen, *Biochemistry 38*, 15278−15286.
24. O'Brien, J. R., Schuller, D. J., Yang, V. S., Dillard, B. D., and Lanzilotta, W. N. (2003) Substrate-induced conformational changes in *Escherichia coli* taurine/α-ketoglutarate dioxygenase and insight into the oligomeric structure, *Biochemistry 42*, 5547−5554.
25. Caldwell, S. R., Newcomb, J. R., Schlecht, K. A., and Raushel, F. M. (1991) Limits of diffusion in the hydrolysis of substrates by the phosphotriesterase from *Pseudomonas diminuta*, *Biochemistry 30*, 7438−7444.
26. Adams, J. A., and Taylor, S. S. (1992) Energetic limits of phosphotransfer in the catalytic subunit of cAMP-dependent protein kinase as measured by viscosity experiments, *Biochemistry 31*, 8516−8522.
27. Cole, P. A., Burn, P., Takacs, B., and Walsh, C. T. (1994) Evaluation of the catalytic mechanism of recombinant human Csk (C-terminal Src kinase) using nucleotide analogs and viscosity effects, *J. Biol. Chem. 269*, 30880−30887.
28. Weast, R. C., Astle, M. J., Beyer, W. H. (1984) *CRC Handbook of Chemistry and Physics*, 64th ed., CRC Press Inc., Boca Raton, FL.

BI050227C